Long-range transport and tropospheric ozone variability in the western Mediterranean region during the Intercontinental Transport of Ozone and Precursors (ITOP-2004) campaign

F. Ravetta,[1] G. Ancellet,[1] A. Colette,[1] and H. Schlager[2]

[1] Two ground-based ozone lidars have been operated at Observatoire de Haute Provence (OHP) for 11 days during the Intercontinental Transport of Ozone and Precursors (ITOP-2004) measurement campaign. Ozone and scattering ratio vertical profiles have been measured from the boundary layer up to the tropopause. At first order, tropospheric ozone temporal variability is due to local pollution within the planetary boundary layer and to stratosphere-troposphere exchange. Remaining ozone rich layers within the free troposphere are related to long-range transport processes. Transport pathways are discussed combining Lagrangian particle dispersion modeling analysis and upstream airborne in situ measurements of the chemical composition of these air masses. High ozone and CO mixing ratios measured within polluted plumes aboard the aircraft correspond to ozone and aerosol layers seen by the lidar. Most of these layers have their origin in North America where they are uplifted either by forest fires or by warm conveyor belts in the vicinity of frontal regions. During the campaign, these polluted and thin (<1 km) layers remain coherent and are transported in a Lagrangian manner over the Atlantic Ocean. The layers observed above OHP in the lower free troposphere exhibit ozone mixing ratio 50% larger than background values. With an ozone content of 3 to 6 Dobson Units, these layers increase by 5 to 10% the background tropospheric ozone column.

Citation: Ravetta, F., G. Ancellet, A. Colette, and H. Schlager (2007), Long-range transport and tropospheric ozone variability in the western Mediterranean region during the Intercontinental Transport of Ozone and Precursors (ITOP-2004) campaign, *J. Geophys. Res.*, *112*, D10S46, doi:10.1029/2006JD007724.

1. Introduction

[2] Given the lifetime of tropospheric ozone (1 to 2 months), photochemical and transport processes, from the local to the synoptic scale, control the variability of its distribution. It is well known that mesoscale processes at midlatitudes (cutoff low, tropopause fold) can bring significant amounts of stratospheric ozone into the free troposphere [*Danielsen*, 1968; *Danielsen et al.*, 1987; *Browell*, 1987; *Vaughan and Price*, 1989; *Price and Vaughan*, 1993]. Specific campaigns [*Ravetta et al.*, 1999; *Ravetta and Ancellet*, 2000] and climatological analysis [*Ancellet and Beekmann*, 1997; *Colette et al.*, 2005] have studied their impact in the western Mediterranean region. This region is also subject to strong photo-oxidant pollution episodes [*Cros et al.*, 2005] and recirculation of polluted air masses [*Millan et al.*, 1996]. Recent studies have shown that long-range transport of pollution can move significant amounts of ozone within the troposphere [*Stohl and Trickl*, 1999]

and that the Mediterranean region is at a crossroad of global air pollution pathways [*Lelieveld et al.*, 2002]. Systematic studies are still needed to estimate the relative impact of each of these processes, especially long-range transport, on the ozone budget [*Brasseur et al.*, 2003].

[3] Within the International Global Atmospheric Chemistry (IGAC) program, the Intercontinental Transport and Chemical Transport (ITCT) project has been set up to quantify the impact of long-range transport on the ozone budget, besides photochemical production and transport from the stratosphere. In relation to ITCT, the Intercontinental Transport of Ozone and Precursors (ITOP-2004) experiment took place in summer 2004 to study American outflow in a quasi Lagrangian manner and to quantify its impact on ozone and aerosol budget in Europe. Several aircraft were involved to follow from a Lagrangian point of view the evolution of air masses while crossing the Atlantic Ocean [*Fehsenfeld et al.*, 2006; *Real et al.*, 2007; *Methven et al.*, 2006]. During ITOP, the ozone lidar station of the Observatoire de Haute-Provence (OHP) has been used to document the variability of the tropospheric ozone field in the western Mediterranean basin.

[4] The OHP data set discussed here consists of semi-continuous measurements of high-resolution vertical ozone profiles, from the boundary layer up to the tropopause, over an intensive observation period of 11 days when airborne in

[1]Service d'Aéronomie, Institut Pierre Simon Laplace/Université Pierre et Marie Curie−Paris 6, Paris, France.
[2]Institut für Physik der Atmosphäre, Deutsches Zentrum für Luft und Raumfahrt, Wessling, Germany.

situ measurements in the flow upstream of the station are available. The goal of this paper is to present this data set and to analyze the variability of the tropospheric ozone field above the OHP during the campaign in order to (1) establish which layers correspond to long-range transport of pollution and (2) discuss the origin of these layers using trajectories calculation and correlation between ozone, carbon monoxide and aerosol content. To what extent these air masses are incorporated within the European boundary layer is not discussed here. This question needs mesoscale modeling studies out of the scope of the article.

[5] The structure of the article is the following. The OHP data set is presented in section 2. The influence of local pollution and stratosphere troposphere exchange (STE) on the tropospheric ozone field is discussed in section 3. Section 4 looks for the origin of the remaining ozone-rich layers which must be related to long-range transport of older polluted air masses. Indeed, these layers are either linked to forest fires plumes (subsection 4.1) or to frontal uplift processes over the American continent (subsection 4.2). Conclusions and perspectives are drawn in section 5.

2. Data Set

[6] The Observatoire de Haute Provence (OHP) is a ground based station equipped with many instruments to sample the atmosphere, including profilers like lidars. OHP is located in southern France (43.9°N, 5.7°E), 690 m above sea level. This study is based on the analysis of tropospheric ozone and aerosol profiles measured at OHP during ITOP. The data set has been built using two ozone lidars in order to characterize both the planetary boundary layer (PBL) and the free troposphere up to the tropopause. The ozone lidar raw data have been processed to derive vertical profiles of two geophysical quantities: the tropospheric ozone mixing ratio and the scattering ratio. Ozone in situ measurements by a standard UV absorption analyzer were also made at the ground. Combining these data sets makes possible the analysis of the ozone vertical distribution from the ground up to the tropopause between 21 and 31 July 2004.

2.1. Instrumentation and Data Processing

[7] The ozone lidar of the OHP [*Ancellet et al.*, 1989], named OHP lidar in this study, is used for ozone monitoring in the troposphere and lower stratosphere (2–3 km above the tropopause at night). It has been operated at OHP since 1990 either for routine measurements twice a week [*Ancellet and Beekmann*, 1997] or in a much more continuous way during specific campaigns like ITOP. Given the overlap between the field of view of its telescope and the divergence of the laser beam, the OHP ozone lidar is blind below an altitude above sea level of 3 km. Between 3 and 4 km a geometric correction has to be applied. This is the reason why during ITOP-2004, the UV-DIAL ozone lidar ALTO (Airborne Lidar for Tropospheric Ozone), named ALTO lidar hereafter, was brought to the station [*Ancellet and Ravetta*, 1998]. When ground-based, this airborne lidar is able to sample tropospheric ozone between 0.6 and 4 km above the ground [*Ancellet and Ravetta*, 2003]. This corresponds here to an altitude range above sea level of 1.3 to 4.7 km.

[8] The two ozone lidars are based on the UV-DIAL technique. At least two wavelengths in the near UV (316

and 289 nm for the OHP lidar, 316, 289 and 266 nm for ALTO lidar), with a large differential absorption cross section by ozone, are emitted into the atmosphere. The backscattered light is collected with a telescope. A spectrometer, several photomultipliers and signal-processing electronics make possible to separate wavelengths, to amplify the signal and to record the raw data into computer files. Both a photocounter and a waveform recorder are used for each wavelength.

[9] The lidar raw signals at the wavelengths needed for the DIAL technique are processed in the same way for both lidars. First, raw data are time averaged to increase the signal-to-noise ratio. The temporal resolution in this study is usually of 30 min for OHP lidar and 10 min for ALTO lidar. The background level is computed using the 250 μs tail of the lidar return signal. The aerosol backscatter coefficient at 316 nm is computed using a backward integration scheme [*Browell et al.*, 1985] and a reference backscatter value taken in the cleanest altitude range where Rayleigh backscatter dominates. The range corrected lidar signals are further averaged using a second-order polynomial fit over a number of points that increases with range. The corresponding vertical resolution of the measurement increases continuously from 300 m at 3-km range to 1200 m at 10-km range for the OHP lidar and from 200 m at 600-m range to 900 m at 4-km range for ALTO lidar. In the range where they are used both instruments are able to detect thin ozone layers (<300 m). The lidar signals are finally corrected for Rayleigh extinction and oxygen extinction, using an atmospheric model [*Ancellet and Ravetta*, 1998]. Differential backscatter and extinction by aerosols are also corrected using the aerosol backscatter profile at 316 nm and a spectral dependency approximated by a power law. The extinction and backscatter wavelength variation between the blue (450 nm) and the green (550 nm) is of the order of λ^{-2} in the free troposphere and λ^{-1} in the PBL according to the in situ measurements of an ultralight aircraft which flew during the ESCOMPTE campaign in summer 2001 in the same area [*Junkermann*, 2005]. The same values were used for all the ozone profiles presented in this paper. An uncertainty remains on the ozone concentrations even after this correction but it will be most important in the heavily polluted PBL or near clouds. Given the averaging process and the correction applied, ozone is finally computed with an uncertainty of about 10% [*Ancellet and Ravetta*, 2005]. Inside clouds or in the very foggy PBL ozone data are not available.

2.2. Ozone Vertical Profile

[10] Figure 1 is an example of the vertical ozone profiles measured by both instruments on 21 July around 1000 UT. An ozonesonde was launched at the same time to provide a reference profile. Even if the ozone lidars and the ozonesonde do not sample the same air masses, especially at high altitude where the sonde drifts away from the vertical, one can notice the overall good agreement between lidar measurements and the ozonesonde, in terms of vertical structures and ozone level. Small discrepancies are within measurement uncertainties. There is also a good agreement between both lidars when they overlap between 3.5 and 4.5 km. The two ozone lidar profiles have usually been joined at an altitude above sea level of 4 km. This is the way Figures 2a, 3a and 4a
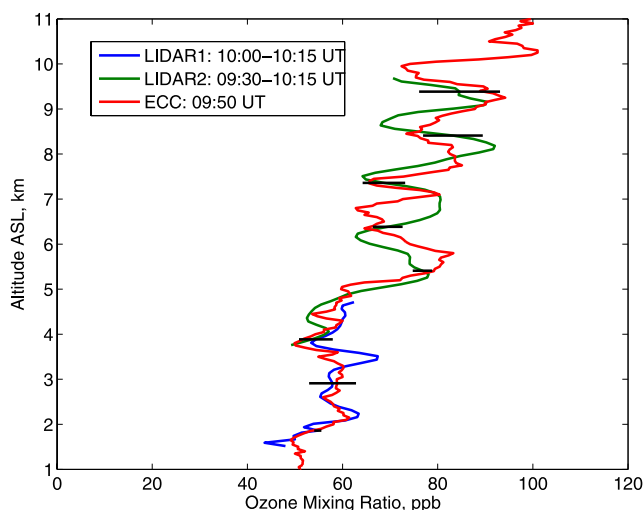
Figure 1. Ozone vertical profile measured at OHP on 21 July 2004 around 1000 UT by an ozonesonde (red line), ALTO lidar (blue line) and OHP lidar (green line) with error bars (horizontal black lines) for lidar measurements plotted at several altitudes.

were built. Figures 2a, 3a, and 4a show all ozone measurements profiles made with OHP and ALTO lidars between 21 and 31 July 2004. Around 4 km, when one switches from one lidar to the other, the vertical profile is usually continuous. This gives confidence in the ozone profile reconstruction developed to avoid instrumental errors related to the low signal-to-noise ratio of the ALTO lidar above 4 km and the nonuniform overlap function of the OHP lidar below 4 km.

2.3. Scattering Ratio

[11] Lidar data inversion at 316 nm, where absorption by ozone can be neglected in the troposphere, makes possible to compute aerosol extinction at this wavelength. Only a qualitative estimate of its vertical distribution can be obtained as an assumption has to be made about the "backscatter to extinction" ratio [Klett, 1981, 1985]. Here again, the range corrected lidar signal at 316 nm is vertically averaged using a second-order polynomial fit, but over a smaller number of points, and vertical resolution increases continuously from 50 m at 600-m range to 100 m at 4 km. The aerosol vertical profile was studied using the scattering ratio, which is the ratio of total backscattering (by molecules and by aerosols) to molecular backscattering.

[12] The scattering ratio is always larger than 1, the value of pure Rayleigh scattering. Figures 2b, 3b and 4b show the
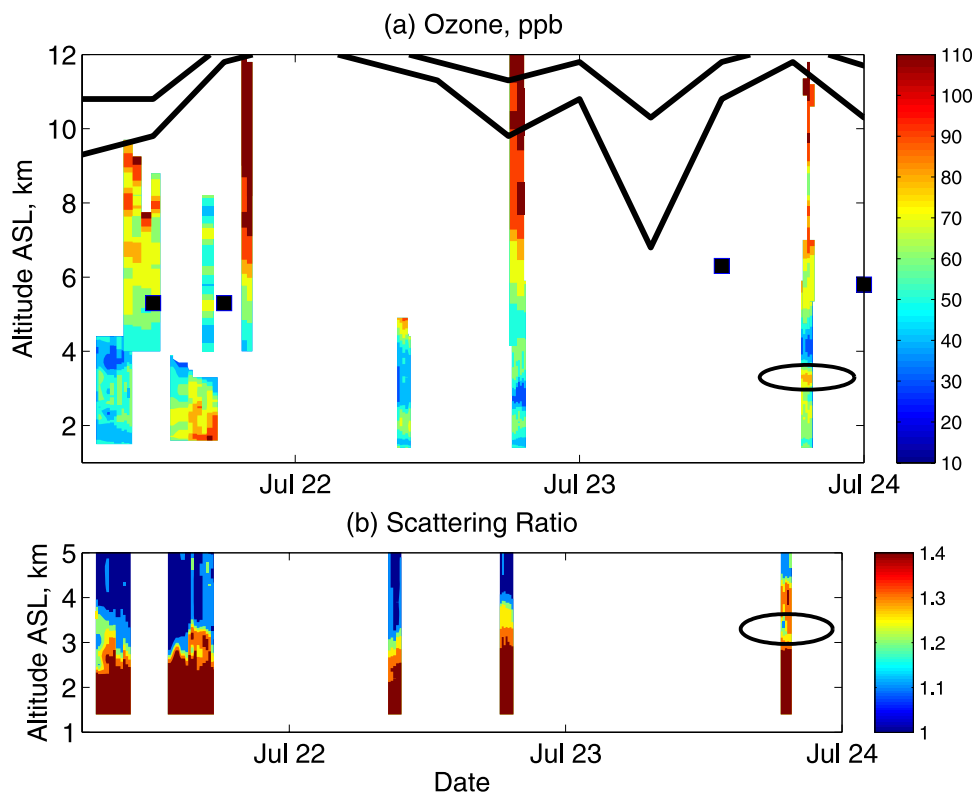

Figure 2. (a) Ozone mixing ratio cross section in ppb measured at OHP on 21, 22 and 23 July 2004. Tick marks correspond to 0000 UT. This picture combines vertical profiles measured by two ozone lidars. ECMWF analyses have been used to compute potential vorticity (PV) profiles in order to estimate the height of the tropopause (PV = 1 pvu for the lower thick black line, PV = 2 pvu for the upper one) and spot stratospheric intrusions (large squares). (b) Scattering ratio vertical cross section derived from the 316-nm wavelength ALTO lidar on the same days. Ozone rich layers related to long-range transport are circled in black.
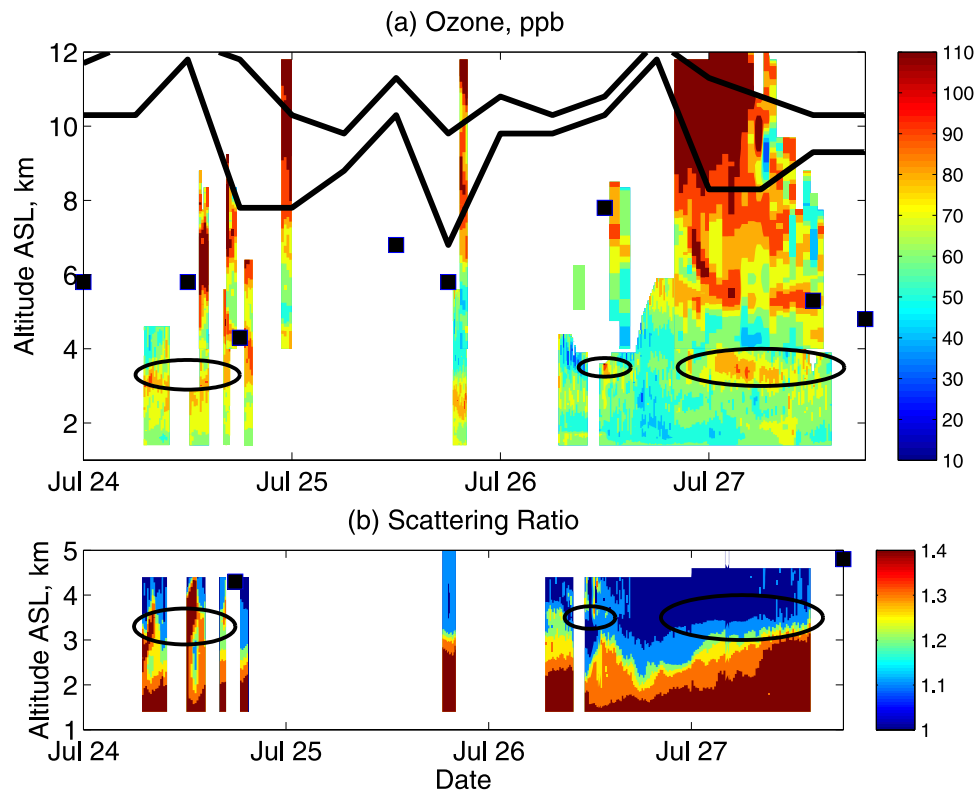
Figure 3. (a and b) Same as Figure 2 on 24, 25, 26 and 27 July 2004.
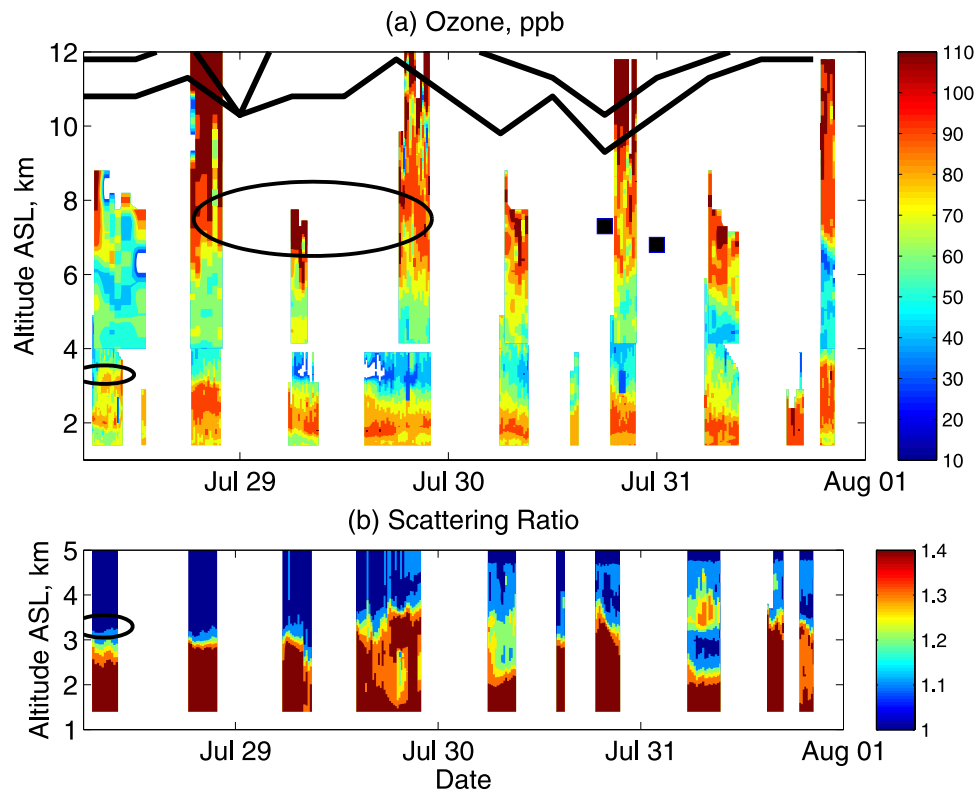

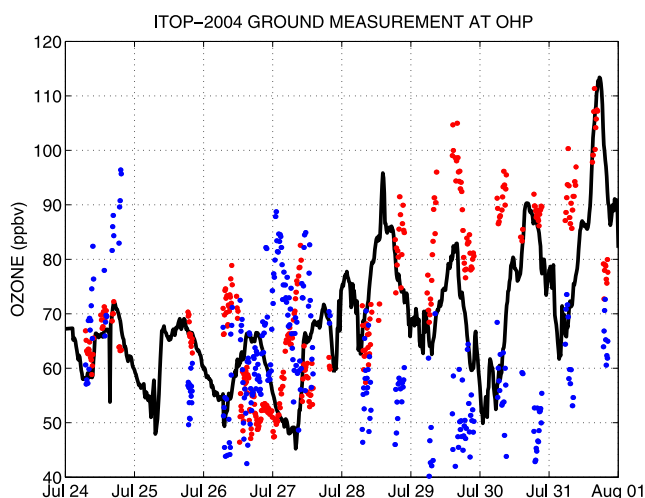**Figure 4.** (a and b) Same as Figure 2 on 28, 29, 30 and 31 July 2004.

Figure 5. Ozone mixing ratio time series at ground level (black line) between 24 July 2004, 0000 UT, and 31 July 2004, 2400 UT. No ground based measurements were made between 21 and 23 July. Red dots are ALTO lidar ozone measurements at an altitude of 1.7 km. Blue dots are ALTO lidar ozone measurements at an altitude of 3.2 km.

distribution of aerosols, in terms of scattering ratios, between 21 and 31 July 2004. Scattering ratio varies between 1.4 and 1.1 in the boundary layer which contains a lot of particles. In the free troposphere scattering ratio is close to 1 for aerosol free air masses. It can be above 1.2 for air masses with a significant aerosol load (polluted air masses for instance). Correlation between ozone and aerosol within ozone rich layers will be discussed below.

3. Ozone Variability: Regional Pollution and STE

[13] Figures 2–4 show the ozone vertical cross section above OHP between 21 and 31 July 2004 from the near ground up to the tropopause, during ITOP intensive observation period. This tropospheric ozone field is highly variable. Before discussing how long range transport of polluted air masses accounts for this variability, it is necessary to identify ozone rich air masses related to local and regional pollution or to stratosphere-troposphere exchange.

3.1. Local Variability and Regional Pollution

[14] In Figures 2–4, the ozone mixing ratio close to the ground peaks above 100 ppb on 21 July and after 28 July. It stays below 70 ppb between 24 and 27 July. The same variability is observed by the ozone monitor at ground level between 24 and 31 July. Indeed Figure 5 shows well-defined diurnal cycles with ozone daily maxima below 75 ppb between 24 and 27 July, above 75 ppb after, even up to 110 ppb on 31 July. The results of an operational chemical and transport model (PREVAIR) designed to forecast predict photo-oxidant pollution episodes over France on a daily basis are consistent with these observations. A day by day analysis of the simulation (see http://prevair.ineris.fr) shows that ozone production related to regional pollution is limited between 21 and 23 July, and that a very strong pollution episode occurs after 27 July. As the variability of the ozone

field within the boundary layer is related to local and regional pollution it will not be further investigated.

[15] In this study, we need to identify ozone or aerosol rich layer above the planetary boundary layer. It can be seen in Figure 5 that the correlation between surface measurements at OHP and ALTO ozone lidar data decreases with altitude. We first used the minimum of the second-order derivative of the lidar range corrected signal at 316 nm to estimate more precisely the height of the boundary layer [*Menut et al.*, 1999]. This method did not provide robust results here. For this reason, we directly used the vertical variation of the scattering ratio to estimate the vertical extension of the boundary layer. Given the usually large amount of aerosols within the boundary layer, this ratio is larger than 1.2 from the ground up to the top of the boundary layer. It is close to 1 in the free troposphere, except within isolated aerosol rich layers located above the top of the boundary layer. Such aerosol rich layers in the free troposphere can for instance be seen in Figures 2 and 3 above 3 km on 23 July and above 2.5 km on 24 July. Ozone values are high within these two layers but it will be established in section 4.1 that their origin is not local. There are also ozone rich layers close to the top of the boundary layer, for instance on 28 July (see Figure 4). However, they are free of aerosol which makes very unlikely any fresh injection from the local boundary layer to account for them. Their origin will be discussed in section 4.2.

3.2. Stratosphere Troposphere Exchange

[16] The influence of stratosphere troposphere exchange (STE) on tropospheric ozone variability at OHP during ITOP has been investigated using potential vorticity (PV) fields computed using the European Center for Meteorological Weather Forecast analyses with a horizontal resolution of $0.5625°$ (T213). PV distributions on isentropic surfaces show that several positive PV anomalies were advected above OHP station during ITOP. Vertical profiles of potential vorticity around the OHP led to the identification of tropopause folds and to the computation of the altitude of the tropopause layer defined here as the layer between 1 and 2 PVu (1 PVu = 10^{-6}K kg^{-1} m^2). Stratospheric ozone and potential vorticity are strongly and positively correlated in the lower stratosphere. In addition PV is a conservative quantity for several days during STE events. It can therefore be used to point tropospheric ozone-rich air masses with a stratospheric origin [*Ertel*, 1942; *Vaughan and Begum*, 1989; *Danielsen*, 1990; *Browell et al.*, 2003]. The tropopause layer and tropopause folds (large squares) are drawn in Figures 2–4. These PV calculation match well most of the ozone-rich layers observed in the free troposphere above an altitude of 5 km. The link between the tropopause fold and the stratospheric reservoir is obvious during the night from 26 to 27 July. On 24 July a tropopause fold is even observed down to an altitude 4.5 km. However, PV from ECMWF analyses does not indicate any stratospheric influence that could explain the ozone rich layer observed in the upper free troposphere on 29 July.

4. Ozone Variability and Long-Range Transport

[17] At this stage we identified six ozone-rich layers whose origin is neither directly influenced by regional pollution nor
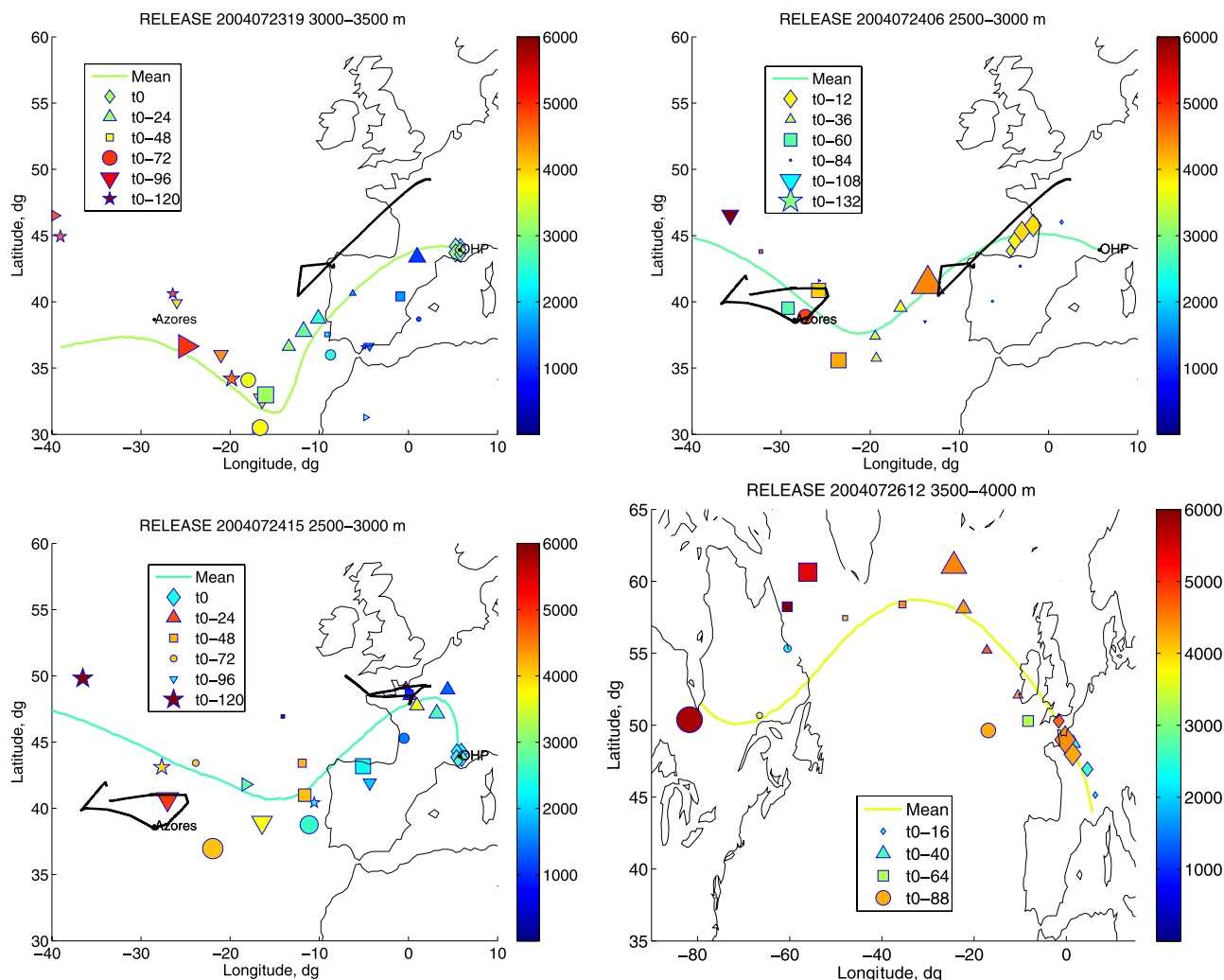
Figure 6. Map of the five FLEXPART cluster positions every 24 hours for particles released from OHP at time t0: (top left) 23 July, 1900 UT, between 3 and 3.5 km; (top right) 24 July, 0600 UT, between 2.5 and 3 km; (bottom left) 24 July, 1500 UT, between 2 and 2.5 km; and 26 July, 1200 UT, between 3.5 and 4 km. The color scale is the altitude of the cluster in m. The size of the clusters corresponds to the number of particles included in the cluster, and the color corresponds to its altitude. The black lines represent the DLR-Falcon flight track on 22 July (top left and right), 23 July (bottom left) and 25 July (bottom right) and the BAe-146 flight track near the Azores on 20 July. The color lines represent the mean positions of the FLEXPART particle plume. Their colors correspond to the altitude of the ending point.

linked to STE. These layers are circled in Figures 2–4. Correlation between ground based ozone and scattering ratio lidar measurements and correlation between airborne in situ ozone and carbon monoxide (CO) measurements will now be used to characterize these air masses. Using airborne lidar and in situ measurements former studies have already proved the effectiveness of this method to constrain the origin of ozone-rich layers [*Browell et al.*, 1996a, 1996b, 2003].

[18] To discuss air mass transport and link ground-based measurements to airborne in situ measurements we use here the Lagrangian Particle Dispersion Model (LPDM) FLEX-PART version 5.1 [*Stohl et al.*, 1998, 2002]. It is driven by 6-hourly ECMWF ERA40 reanalyses (T106L60) inter-leaved with operational forecasts every 3 hours. In addition to classical advection, the LPDM includes turbulent diffu-sion, parameterizations of subgrid-scale convection and of topographic processes. Working with large numbers of trajectories makes also the discussion of transport more robust than using single back trajectories. In addition, online computation of potential vorticity for each air parcel is available making it possible to check any stratospheric influence.

[19] Investigating the six layers, it was not possible to link the air mass observed on 29 July in the upper troposphere to any airborne measurements. Transport anal-ysis shows that this air mass remained in the upper troposphere for at least 5 days without experiencing any significant stratospheric influence. It is very likely to correspond to long-range transport of an old polluted air mass but we were not able to clearly identify its origin. We
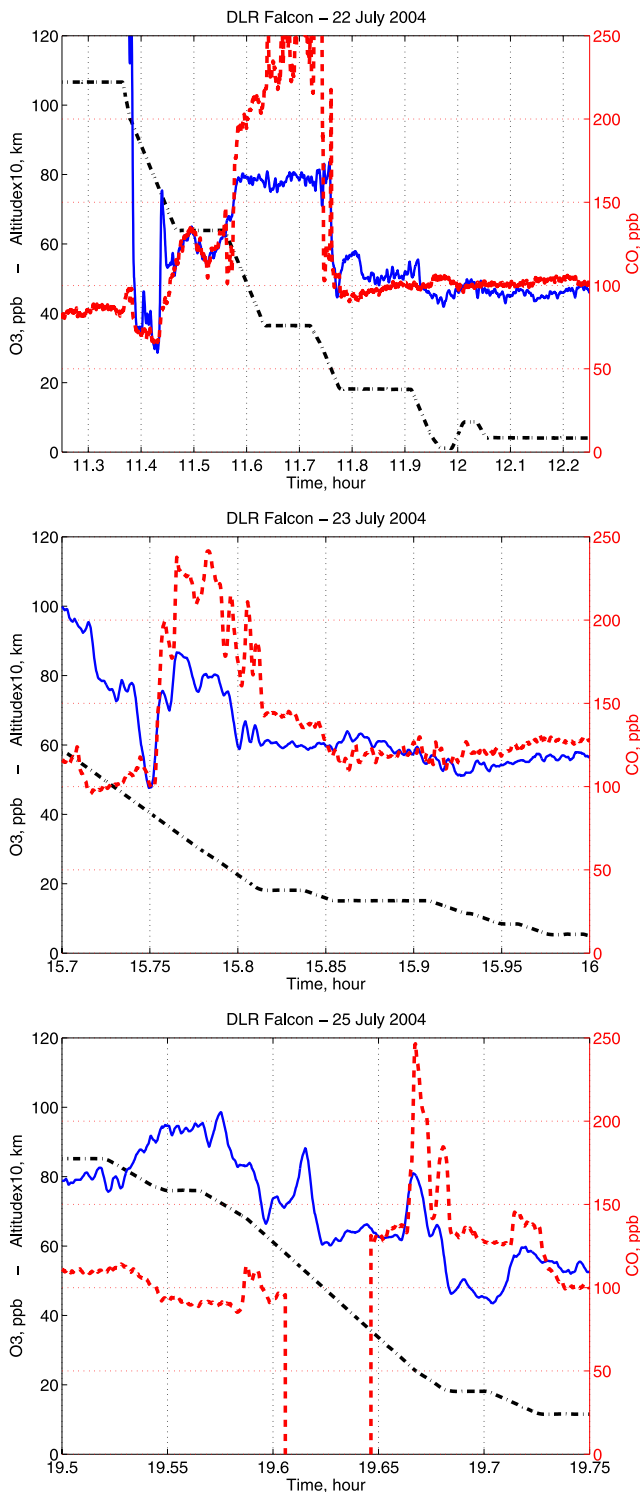
Figure 7. Time evolution of the DLR-Falcon O$_3$ (solid line) and CO (dashed line) concentrations during descent (top) to the Spanish coast on 22 July, 1200 UT, and to Paris on (middle) 23 July, 1600 UT, and (bottom) 25 July, 1930 UT. Altitude (dashed-dotted line) in km is multiplied by 10 on left scale.

will thus focus on the five remaining layers. All these layers belong to the 3- to 5-km altitude range and exhibit ozone values above 75 ppb (up to 90 ppb), at least 50% larger than the 40–50 ppb background values. These layers are 500 m to 1 km thick and thus correspond to an ozone content of 3 to 6 DU, accounting for 10 to 20% of the tropospheric ozone burden.

4.1. Long-Range Transport: Forest Fire Plumes

[20] Among the selected ozone-rich layers related to long-range transport, three are associated to aerosol scattering ratio at 316 nm above 1.2: (1) at 3–3.5 km on 23 July, 1900 UT; (2) at 2.5–3.5 km on 24 July, from 0600 UT to 1600 UT; and (3) at 3–4 km on 26 July, 1200 UT. We will here examine whether these layers can be related to forest fire plumes.

[21] Using FLEXPART, 2000 particles were released in the vicinity of a detected ozone-rich layer during 30 min in a volume of 500-m depth and $1° \times 1°$ horizontal surface. The dispersion of this air parcel was then computed for 5 days backward in time. As we focus on layers, our aim is to document their history as long as they remain coherent, i.e., before they undergo strong mixing which, as reported by *Methven et al.* [2003], becomes significant after 3.3 ± 0.6 days for trajectories arriving above western Europe.

[22] At each time step, the 2000 air parcels are clustered into 5 bins depending on their geographical location [*Stohl et al.*, 2005]. In order to provide a synthetic chart, the centers of the five clusters are plotted in Figure 6, rather than the positions of the 2000 particles. When the layer remains coherent the five clusters (or at least the largest ones) stay close to each other. Clusters are plotted every 24 hours and are compared to the position of the DLR Falcon or the British BAe-146 aircraft flight tracks. After 4–5 days the dispersion of the cluster is sometimes too large to identify a direct link with the ozone precursor source region. One can discuss instead the link with aircraft observations in Europe or above the Atlantic ocean, especially using CO mixing ratio which is known to be very high in air masses polluted by biomass burning. PV values of the clusters are never higher than 1 PVu (not shown) for the time evolution shown in Figure 6. According to the LPDM only few particles may have been uplifted less than 1 day before from the European PBL on 23 and 24 July above central France or northern Spain, at a time when local photochemical production is too low to explain the high observed ozone values (section 3.1). One can also notice that for the air masses arriving at OHP on 24 July, 1500 UT, the geographical dispersion of the clusters is already significant 3 days before. This is related to the fact that after noon on 24 July at OHP a tropopause fold is starting to cap the pollution layer located between 2.5 and 3.5 km (see Figure 2 and *Cho et al.* [2001] for an example of such a capping process). Both layers have very different origins. Indeed the LPDM simulation for the 3.5–4 km layer indicates that some particles (>10%) are already coming from the stratosphere, i.e., with PV >1.5 PVu (not shown). These results are consistent with the conclusions drawn in section 3 and gives some confidence in the reliability of the LPDM for identifying the origin of the ozone-rich layers observed at OHP.
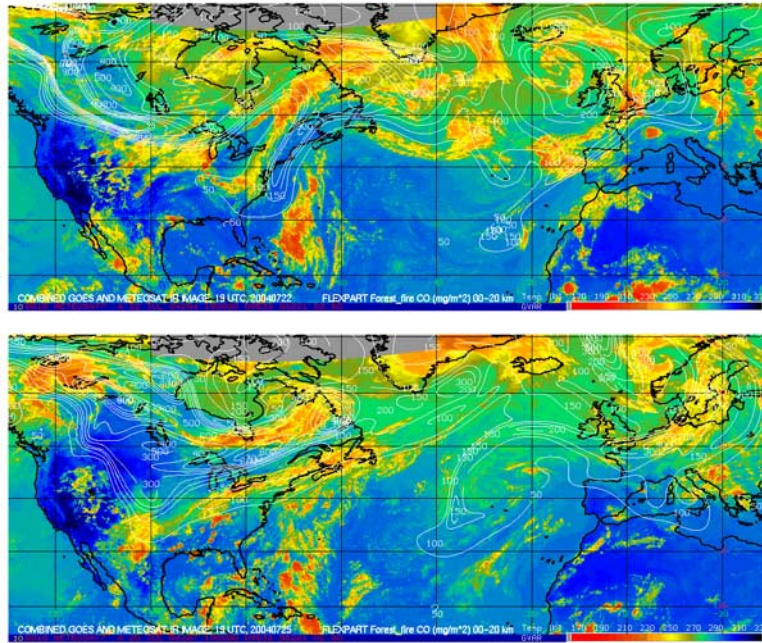
Figure 8. Isoconcentration (thin white lines) of FLEXPART forest fire CO column between 0 and 20 km in mg/m^2 on (top) 22 July, 1900 UT, and (bottom) 25 July, 1900 UT. Cloud brightness temperature is color-coded (red is 220 K).

[23] The LPDM shows that the pollution plume observed at OHP on 24 July between 0600 and 1600 UT must have been sampled by the DLR aircraft. The CO and ozone measured on 22 July off the coast of Portugal and on July during its descent to Paris are plotted in Figure 7 (top and middle). In both cases, an ozone and CO-rich air mass is sampled near an altitude of 4 km. The ozone values measured aboard the DLR aircraft are of the order of 80 ppb within these layers, in good agreement with the lidar observations made less than 24 hours later. CO mixing ratio is above 200 ppb, which is clearly the signature of pollution.

[24] For the air masses arriving at OHP on 24 July, the LPDM also indicates a link with a forest fire plume located west of the Portuguese coast on 22 July in the late afternoon and identified by the FLEXPART forest fire CO simulations computed by NOAA and available on the ICARTT web site http://www.esrl.noaa.gov/csd/metproducts/icartt2004/ (Figure 8). The DLR Falcon actually sampled the northern part of this plume at noon on 22 July near an altitude of 4 km, and part of the same air mass 1 day later above northern France below 4 km, since this air mass was subsiding while traveling from the Azores to southern France. Here, the FLEXPART forest fire CO simulation does not provide the altitude of the pollution plume. However, the value, vertically integrated between 0 and 20 km, of simulated forest fire CO is of the same order of magnitude (about 150 mg.m^{-2}) than the CO column measured aboard the DLR aircraft, within the pollution plume and above background values. It is thus consistent to link the pollution plume observed at OHP and sampled aboard the DLR aircraft to this simulated forest fire plume.

[25] The backward LPDM simulations of Figure 6 also suggest that the forest fire plume observed at OHP on 24 July

at 0600 and 1500 UT has been sampled above the Azores by the BAe-146 on 20 July. Indeed, in situ measurements aboard this aircraft show CO data larger than 200 ppb at an altitude of 5 km (see Figure 9). One can investigate this feature by performing forward LPDM simulations from the high CO region identified by the aircraft on 20 July. Two simulations were performed using two boxes of 500-m depth and located just above and just below the 5-km altitude where the pollution plume is observed. The lower air parcels reach OHP below 3 km at 0600 UT on 24 July while the upper ones arrive at 1500 UT. Since ozone values measured by the BAe-146 in the pollution plume are 10-ppb lower than the lidar and DLR Falcon observations 3–4 days later, this gives an upper limit estimate of ozone production within the forest fire plume of 3 ppb per day (see *Real et al.* [2007] for a discussion of photochemical production within forest fire plumes).

[26] Regarding the layer observed at OHP on 26 July, 1200 UT, the LPDM indicates that this air mass has also been sampled by the DLR aircraft during its descend to Paris on 26 July around 1900 UT. Indeed, in situ measurement exhibit an CO peak, positively correlated with ozone around an altitude of 2.5 km. Unfortunately CO data are not available at 4 km where another ozone peak is observed. However, it is still reasonable to make a link with the forest fire plume simulated by FLEXPART on 25 July in the late afternoon above northern France (Figure 8, bottom). Here, as transport above the northern Atlantic is much faster for the air mass observed at OHP on 26 July than on 24 July, a direct link with the forest fire above Canada can be established. Figure 6 (bottom right) shows a strong coherent cluster south of the Hudson Bay on 22 July, where and when a forest fire CO plume is present at this location as shown by the FLEXPART simulation in Figure 8 (bottom).
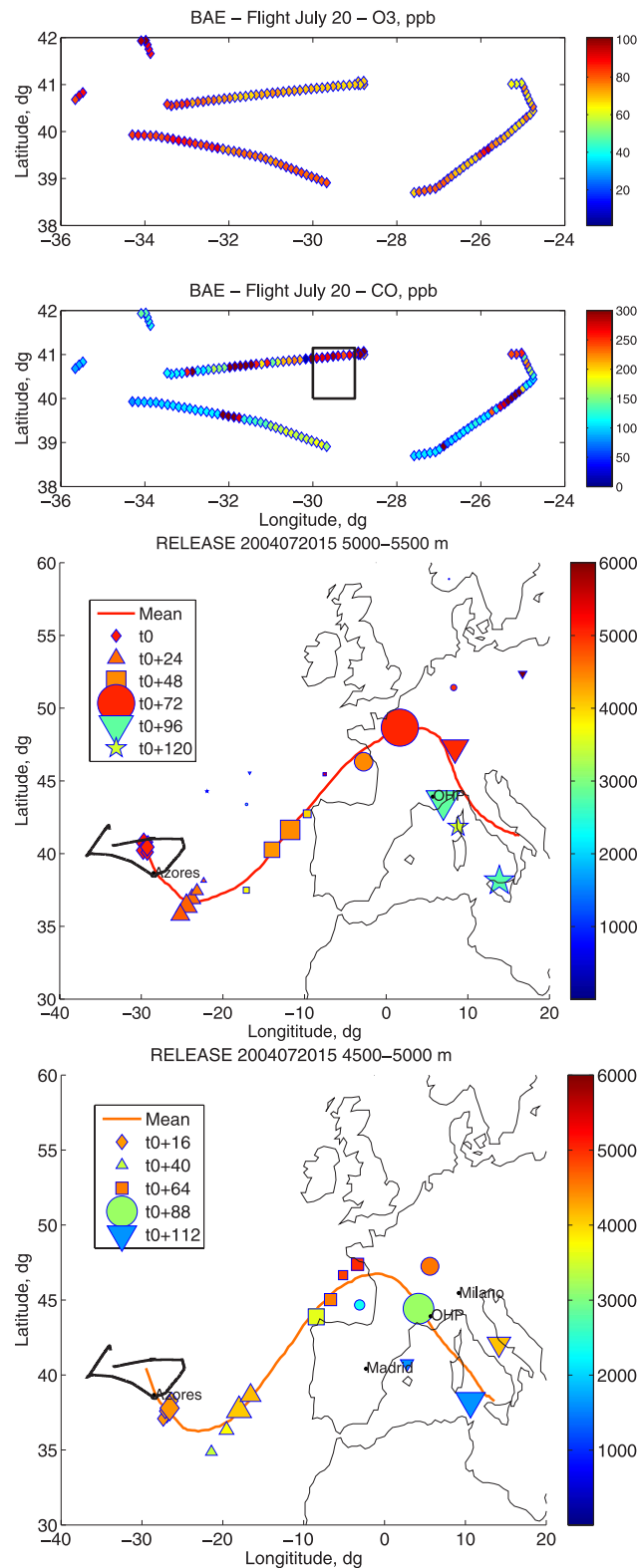
Figure 9. (top) Horizontal distribution at the 5-km altitude of O_3 and CO concentration measurement by the BAe aircraft near the Azores on 20 July. Map of the five FLEXPART cluster positions advected forward every 24 hours for particles released in the black square shown in the top plot on 20 July, 1500 UT, (middle) between 5 and 5.5 km and (bottom) between 4.5 and 5 km. See caption of Figure 6 for more details.

[27] Regarding the layer observed at OHP on 23 July at 1900 UT, observations at OHP are very similar to those made on 24 July with a clear positive correlation between ozone and aerosol load. LPDM analysis (Figure 6, top left) also indicates a possible link with the simulated forest fire CO plume east of Portugal (Figure 8, top). However, it was not possible to use any aircraft data to confirm this hypothesis.

4.2. Long-Range Transport: Frontal Uplift of Polluted Air Masses

[28] Two layers located in the free troposphere have also ozone concentrations larger than 75 ppb without any enhancement of PV values. However, these layers do not exhibit any enhancement of the aerosol scattering ratio. Therefore their origin is different from the layers investigated in section 4.1. These layers are observed (1) at $3-4$ km on 27 July during the night from 0100 to 0600 UT and (2) at $3-3.5$ km on 28 July, 0900 UT. Three questions arise from these observations. Are these layers related to long-range transport or regional pollution? Are these layers related to ozone sources from North America? If yes, why no detectable aerosol signature is seen in the lidar observations?

[29] Again using FLEXPART, 2000 particles were released at $3.5-4$ km on 27 July 0300 UT and at $3-3.5$ km on 28 July 0900 UT. Backward plume dispersions are shown in Figure 10. The LPDM simulations show the same kind of transport pathway for both air masses: uplifting from the North American continent up to $5-6$ km and turning around the high-pressure system above North Atlantic before subsiding in the $3-4$ km altitude range above southern France. Considering the strong subsidence associated to the northerly flow, the influence of European emission above 3 km is discarded: these air masses are not linked to regional pollution.

[30] Advection is slightly faster for the 27 July layer. Both layers were uplifted from the same area above North America, namely between Montréal and the Great Lakes. For the 28 July layer, the cluster is well defined below 3 km and close to Montreal on 22 July at 2200 UT (t0-132). For the 27 July layer, the plume is more scattered on 22 July at 1900 UT (t0-104), but it is still coming from the Great Lakes area.

[31] Since the LPDM shows an uplifting of air masses southwest from the Montreal area in the evening of 22 July, it is interesting to consider the 1900 UT FLEXPART North American CO simulations computed by NOAA and available on the ICARTT web site http://www.al.noaa.gov/metproducts/icartt2004/ (see Figure 11). A high CO plume between 0 and 3 km is clearly observed between the Great Lakes and the northeastern American coast. Furthermore, between Lake Ontario and Montreal, this CO plume corresponds to the southern tip of a cloudy area typical of a warm conveyor belt (WCB) [*Cooper et al.*, 2001]. These features provide a consistent explanation of the origin of both layers: pollution took place in the North American boundary layer, it was uplifted on 22 July and transported above the Atlantic by a WCB.

[32] Contrary to the layers studied in section 4.1, a link with the DLR Falcon or the BAe aircraft could not be established and no information is available on the CO concentrations in the layers observed above OHP.
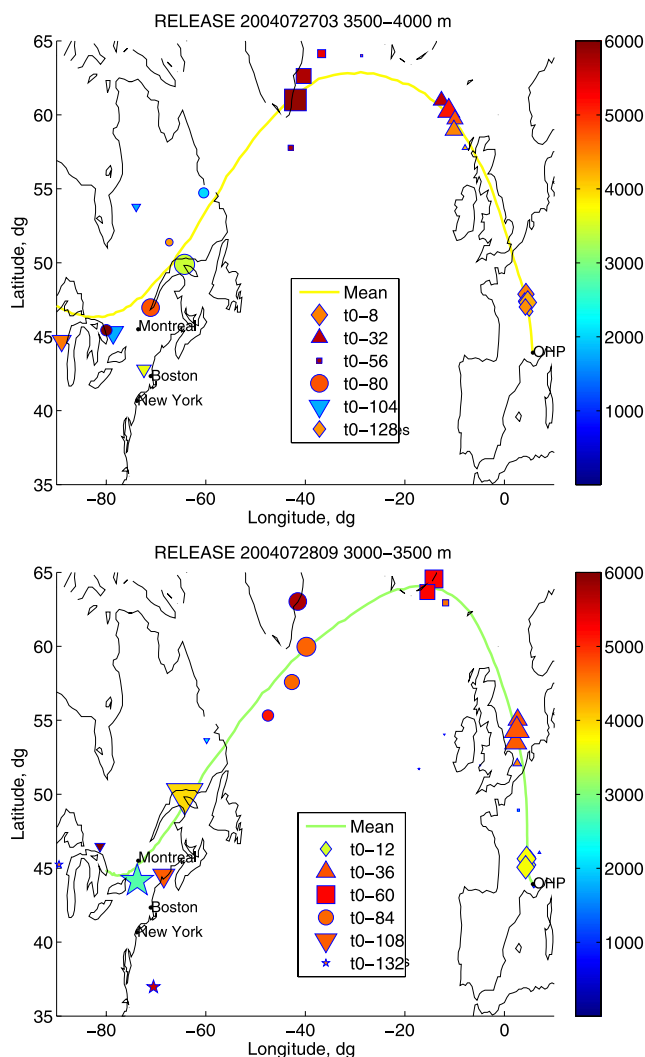
Figure 10. Map of the five FLEXPART cluster positions every 24 hours for particles released from OHP at time to: (top) 27 July, 0300 UT, between 3.5 and 4 km and (bottom) 28 July, 0900 UT, between 3 and 3.5 km. Both t0-104 (top plot) and t0-132 (bottom plot) correspond to the evening of 22 July. See caption of Figure 6 for more details.

Moreover, no American aircraft has flown in this air mass on 22 July. However, the westernmost lag of the P3 flight was located at 73°W, 42°N, 1000 m, 2000 UT above the North American continent and recorded ozone values of the order of 80 ppb with CO values larger than 200 ppb. This confirms that pollution was significant in the continental boundary layer on 22 July.

[33] To strengthen the hypothesis of a North American origin of the air masses observed at OHP, forward LPDM was used to check the fate of the polluted CO air mass uplifted by the WCB over Canada on 22 July (Figure 11). Indeed the 2000 particles released in a $1° \times 1°$ box near Montréal at 2.5–3 km form a plume of polluted air mass arriving in southern France on 27 July after 0000 UT. The spreading of the clusters at 27 July, 0300 UT (t0 + 104), along the transport pathway from Corsica to Central France, also explains the fact that its signature is still detected at OHP 1 day later on 28 July.

[34] Finally, a high positive correlation between ozone and aerosols is usually found in association with continental pollution plumes [*Browell et al.*, 1996a, 1996b, 2003]. Here, transport by a WCB can account for the negative correlation between ozone and aerosol within the plume (see Figures 3 and 4). Indeed, washout must have taken place within this cloudy region. This provides a possible explanation for the low aerosol signature observed by lidar. Aerosol can be removed from the air mass while gases with low solubility like CO, NO_x and O_3 remain at concentrations well above background values.

5. Conclusions

[35] During ITOP, ozone vertical profiles have been measured at OHP, from the near ground up to the tropopause, in a semicontinuous way between 21 and 31 July 2004. This "high-resolution" data set shows that the tropospheric ozone field is highly inhomogeneous and that strong layering in the free troposphere is observed most of the time in July over southern France. These observations are consistent with former ozone climatological studies in the region [*Ancellet and Beekmann*, 1997; *Colette and Ancellet*, 2005] and with the view that quasi-horizontal trace constituents layers are ubiquitous in the troposphere [*Newell et al.*, 2000; *Thouret et al.*, 2000].

[36] For this data set, tropospheric ozone variability was mostly linked to regional pollution episodes within the boundary layer. In the upper troposphere, above an altitude of 5 km, STE drives most of ozone variability, except on 29 July. Below 5 km, in the lower free troposphere, five ozone rich layers are related to long-range transport. These layers are at the mesoscale with a thickness of several hundred meters and a horizontal extension of the order of 100 km estimated from horizontal advection. Using correlation between tracers (ozone and aerosol content derived from lidar measurements, ozone and CO airborne measurements in the flow upstream) and a LPDM, it has been shown that polluted air masses related to North American boundary layer pollution and forest fires remain coherent enough to significantly modulate tropospheric ozone variability in the western Mediterranean region. Correlation between ozone and aerosol profiles provided by the lidar observations are very comparable to the correlation between ozone and CO observed by the DLR Falcon. This offers interesting perspectives for identifying long-range transport of polluted air masses in the free troposphere compared to STE events, when using long-term observations by lidar.

[37] Within these plumes ozone mixing ratio is 50 to 100% larger than in the background troposphere. A 1-km thick polluted layer will thus increase the ozone column by 50% in the 3- to 5-km altitude range and by 10% in the whole troposphere. These low-level tropospheric air masses are important when looking at the impact of long-range transport of polluted air masses on European air quality as they are more likely to mix with the European boundary layer than upper tropospheric air masses. To address this issue a mesoscale model combining chemical and transport processes is mandatory. The use of such a model would also make it possible to study the radiative impact of layering (in terms of aerosol, water vapor and ozone) on mesoscale
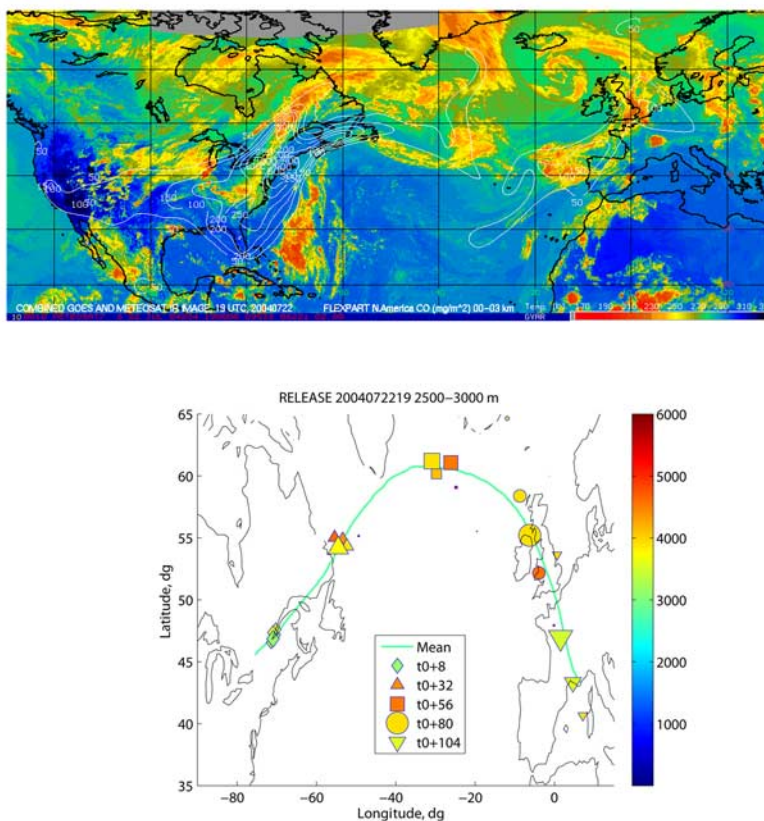
Figure 11. (top) Isoconcentration (thin white lines) of FLEXPART North American CO column between 0 and 3 km in mg/m^2 on 22 July, 1900 UT. Cloud brightness temperature is color-coded. (bottom) Map of the five FLEXPART cluster positions advected forward every 24 hours for particles released in a $1° \times 1°$ box in the North American CO maxima and the ascending branch of the WCB at 45°N, 74°W on 22 July, 1900 UT, between 2.5 and 3 km. Clusters at t0 + 104 correspond to 27 July, 0300 UT.

dynamics. The present study paves the way for such investigations.

References

Ancellet, G., and M. Beekmann (1997), Evidence for changes in the ozone concentration in the free troposphere over southern Europe from 1976–1995, *Atmos. Environ.*, *31*(17), 2835–2851.

Ancellet, G., and F. Ravetta (1998), A compact airborne lidar for tropospheric ozone (ALTO): Description and field measurements, *Appl. Opt.*, *37*, 5509–5521.

Ancellet, G., and F. Ravetta (2003), On the usefulness of an airborne lidar for O$_3$ layer analysis in the free troposphere and the planetary boundary layer, *J. Environ. Monit.*, *5*, 47–56.

Ancellet, G., and F. Ravetta (2005), Analysis and validation of ozone variability observed by lidar during the ESCOMPTE-2001 campaign, *Atmos. Res.*, *74*, 435–460.

Ancellet, G., A. Papayannis, J. Pelon, and G. Megie (1989), DIAL tropospheric ozone measurement using a Nd:YAG laser and the Raman shifting technique, *J. Atmos. Oceanic Technol.*, *6*(5), 832–839.

Brasseur, G., R. Prinn, and A. Pszenny (2003), Atmospheric Chemistry in a Changing World, Springer, New York.

Browell, E. (1987), Tropopause fold structure determined from airborne lidar and in situ measurements, *J. Geophys. Res.*, *92*(D2), 2112–2120.

Browell, E., S. Ismail, and S. Shipley (1985), Ultraviolet DIAL measurements of O$_3$ profiles in regions of spatially inhomogeneous aerosols, *Appl. Opt.*, *24*(17), 2827–2836.

Browell, E., et al. (1996a), Large-scale air mass characteristics observed over western Pacific during summertime, *J. Geophys. Res.*, *101*(D1), 1691–1712.

Browell, E., et al. (1996b), Ozone and aerosol distributions and air mass characteristics over the South Atlantic basin during the burning season, *J. Geophys. Res.*, *101*(D19), 24,043–24,068.

Browell, E., et al. (2003), Ozone, aerosol, potential vorticity, and trace gas trends observed at high latitudes over North America from February to May 2000, *J. Geophys. Res.*, *108*(D4), 8369, doi:10.1029/2001JD001390.

Cho, J., R. Newell, E. Browell, W. Grant, C. Butler, and M. Fenn (2001), Observation of pollution plume capping by a tropopause fold, *Geophys. Res. Lett.*, *28*, 3243–3246.

Colette, A., and G. Ancellet (2005), Impact of vertical transport processes on the tropospheric ozone layering above Europe. Part II: Climatological analysis of the past 30 years, *Atmos. Environ.*, *39*, 5423–5435.

Colette, A., G. Ancellet, and F. Borchi (2005), Impact of vertical transport processes on the tropospheric ozone layering above Europe. Part I: Study of air mass origin using multivariate analysis, clustering and trajectories, *Atmos. Environ.*, *39*, 5409–5422.

Cooper, O., et al. (2001), Trace gas signatures of the airstreams within North Atlantic cyclones: Case studies from the North Atlantic Regional Experiment (NARE'97) aircraft intensive, *J. Geophys. Res.*, *106*(D6), 5437–5456.

Cros, B., et al. (2005), The ESCOMPTE program: An overview, *Atmos. Res.*, *74*, 461–475.

Danielsen, E. (1968), Stratospheric-tropospheric exchange based on radiactivity, ozone and potential vorticity, *J. Atmos. Sci.*, *25*, 502–518.

Danielsen, E. (1990), In defense of Ertel's potential vorticity and its general applicability as a meteorological tracer, *J. Atmos. Sci.*, *47*(16), 2013–2020.

Danielsen, E., R. Hipskind, S. Gaines, G. Sachse, G. Gregory, and G. Hill (1987), Three dimensional analysis of potential vorticity associated with tropopause folds and observed variations of ozone and carbon monoxide, *J. Geophys. Res.*, *92*(D2), 2103–2111.

Ertel, H. (1942), Ein neuer hydrodynamisher wirbelsatz, *Meteorol. Z.*, *59*, 271–281.

Fehsenfeld, F. C., et al. (2006), International Consortium for Atmospheric Research on Transport and Transformation (ICARTT): North America to Europe—Overview of the 2004 summer field study, *J. Geophys. Res.*, *111*, D23S01, doi:10.1029/2006JD007829.

Junkermann, W. (2005), The actinic UV-radiation budget during the ESCOMPTE campaign 2001: Results of airborne measurements with the microlight research aircraft D-MIFU, *Atmos. Res.*, *74*, 461–475.

Klett, J. (1981), Stable analytical inversion solution for processing lidar returns, *Appl. Opt.*, *20*, 211–220.

Klett, J. (1985), Lidar inversion with variable backscatter/extinction ratios, *Appl. Opt.*, *24*(11), 1638–1643.

Lelieveld, J., et al. (2002), Global air pollution crossroads over the Mediterranean, *Science*, *298*, 794–799.

Menut, L., C. Flamant, J. Pelon, and P.-H. Flamant (1999), Urban boundary-layer determination from lidar measurements over the Paris area, *Appl. Opt.*, *38*, 945–954.

Methven, J., S. Arnold, F. O'Connor, H. Barjat, K. Dewey, J. Kent, and N. Brough (2003), Estimating photochemically produced ozone throughout a domain using flight data and a Lagrangian model, *J. Geophys. Res.*, *108*(D9), 4271, doi:10.1029/2002JD002955.

Methven, J., et al. (2006), Establishing Lagrangian connections between observations within air masses crossing the Atlantic during the International Consortium for Atmospheric Research on Transport and Transformation experiment, *J. Geophys. Res.*, *111*, D23S62, doi:10.1029/2006JD007540.

Millan, M., R. Salvador, E. Mantilla, and B. Artinano (1996), Meteorology and photochemical air pollution in southern Europe: Experimental results from EC research projects, *Atmos. Environ.*, *30*, 1909–1924.

Newell, R., V. Thouret, J. Cho, P. Stoller, A. Marenco, and H. Smit (2000), Ubiquity of quasi-horizontal layers in the troposphere, *Nature*, *398*, 316–319.

Price, J., and G. Vaughan (1993), The potential for stratosphere-troposphere exchange in cut-off low systems, *Q. J. R. Meteorol. Soc.*, *119*, 343–365.

Ravetta, F., and G. Ancellet (2000), Identification of dynamical processes at the tropopause during the decay of a cut-off low using high resolution airborne lidar ozone measurements., *Mon. Weather Rev.*, *128*, 3252–3267.

Ravetta, F., G. Ancellet, J. Kowol-Santen, R. Wilson, and D. Nedeljkovic (1999), Ozone, temperature and wind field measurements in a tropopause fold: Comparison with a mesoscale model simulation, *Mon. Weather Rev.*, *127*, 2641–2653.

Real, E., et al. (2007), Processes influencing ozone levels in Alaskan forest fires plumes during long-range transport over the North Atlantic, *J. Geophys. Res.*, *112*, D10S41, doi:10.1029/2006JD007576.

Stohl, A., and T. Trickl (1999), A textbook example of long-range transport: Simultaneous observation of ozone maxima of stratospheric and North American origin in the free troposphere over Europe, *J. Geophys. Res.*, *104*, 30,445–30,462.

Stohl, A., M. Hittenberger, and G. Wotawa (1998), Validation of the Lagrangian particle dispersion model FLEXPART against large scale tracer experiment data, *Atmos. Environ.*, *32*, 4245–4264.

Stohl, A., S. Eckhardt, C. Forster, P. James, N. Spichtinger, and P. Seibert (2002), A replacement for simple back trajectory calculations in the interpretation of atmospheric trace substance measurements, *Atmos. Environ.*, *36*, 4635–4648.

Stohl, A., C. Forster, A. Frank, P. Seibert, and G. Wotawa (2005), Technical note: The Lagrangian particle dispersion model FLEXPART version 6.2, *Atmos. Chem. Phys.*, *5*, 2461–2474.

Thouret, V., J. Cho, R. Newell, A. Marenco, and H. Smit (2000), General characteristics of tropospheric trace constituent layers observed in the MOZAIC program, *J. Geophys. Res.*, *105*, 17,379–17,392.

Vaughan, G., and D. Begum (1989), Correlation between total ozone and potential vorticity, in *Ozone in the Atmosphere*, edited by R. Bojkov and P. Fabian, pp. 91–94, A. Deepak, Hampton, Va.

Vaughan, G., and J. Price (1989), Ozone transport into the troposphere in a cut-off-low episode, in *Ozone in the Atmosphere*, edited by R. Bojkov and P. Fabian, pp. 415–418, A. Deepak, Hampton, Va.

G. Ancellet, A. Colette, and F. Ravetta, Service d'Aéronomie, IPSL/Université Pierre et Marie Curie–Paris 6, F-75252 Paris, France. (francois.ravetta@aero.jussieu.fr)

H. Schlager, Institut für Physik der Atmosphäre, Deutsches Zentrum für Luft und Raumfahrt, D-82230 Wessling, Germany.